Supplement of Atmos. Chem. Phys., 23, 5835–5850, 2023
https://doi.org/10.5194/acp-23-5835-2023-supplement

Atmospheric Chemistry and Physics
Open Access
EGU

Supplement of

Changes in global teleconnection patterns under global warming and stratospheric aerosol intervention scenarios

Abolfazl Rezaei et al.

Correspondence to: Abolfazl Rezaei (arezaei@iasbs.ac.ir, abolfazlrezaei64@gmail.com)

Contents of this file:

Table S1 and Figures S1 to S7.

Introduction

Table 1 and the following figures illustrate the supporting results mentioned in the manuscript as follows:

Table S1. The global-mean values of SST, JJA land temperature minus historical, precipitation, and ECS simulated by CESM1 and CESM2 relative to the historical values over the 1985-2014 period (modified after Danabasoglu et al., 2020).

Figure S1. Box and whiskers plot of the variance in the leading EOFs, representing AMO, PDO, and ENSO, relative to the total variance of the SST fields: AMO across the North Atlantic (top row); ENSO (middle row) global SST; and PDO across the North Pacific (bottom row). The values in blue on each column box show the period of the data for historical, greenhouse gas (i.e., RCP-8.5 and SSP5-8.5), and climate intervention (GLENS-SAI and SSP5-8.5-SAI) scenarios. The titles of each subplot refer to the CESM version and the number of ensembles used in the historical, greenhouse gas (RCP8.5 and SSP5-8.5), and SAI (GLENS-SAI or SSP5-8.5-SAI) scenarios, respectively. The median for each experiment is denoted by the red line, the upper (75^{th}) and lower (25^{th}) quartiles by the top and bottom of the box and ensemble limits by the whisker extents. The three values shown in bottom of each sub-plot refer to the p-values obtained from statistical t-test between historical and global warming, historical and SAI, and global warming and SAI, respectively, in which the underlined values are significant (i.e., $p<0.05$).

Figure S2. The first EOF (1EOF) modes of global SST anomaly relate to the ENSO index under the CESM1 for the historical data and the three ensemble members (001 to 003) outputs from the RCP8.5 and GLENS-SAI scenarios.

Figure S3. As in Fig. S2, but for the CESM2.

Figure S4. Comparison between spatial leading mode of SST anomaly (related to ENSO) form (a) observation data, (b) CESM1, and (c) CESM2 over the historical 1980-2009 period.

Figure S5. The wavelet power spectrum WPS (left column) and global wavelet spectrum GWS (right column) of ENSO obtained from CWT for the (a and b) historical, (c and d) SSP5-8.5, and (e and f) SSP5-8.5-SAI scenarios.

Figure S6. As Fig. 8 but obtained from the concatenated members of the CESM2 historical simulations.

Figure S7. Comparison of the spatial patterns of the first EOF SST ENSO-anomaly from the observations (i.e., measurements) and the CESM1 and CESM2 over the historical 1980-2009 period.

Table S1. The global-mean values of SST, JJA land temperature minus historical, precipitation, and ECS simulated by CESM1 and CESM2 relative to the historical values over the 1985-2014 period (modified after Danabasoglu et al., 2020).

Variable	SST (°C) over 1985-2014	JJA land T (°C) minus historical (1985-2014)	Precipitation(mm/d) over 1985-2014	ECS (°C)
Historical	18.29	-	2.69	1.5 – 4.5
CESM1	18.02	-0.99	3.02	4.0
CESM2-WACCAM	18.63	0.25	2.92	5.1
CESM2-CAM6	18.69	0.37	2.94	5.3

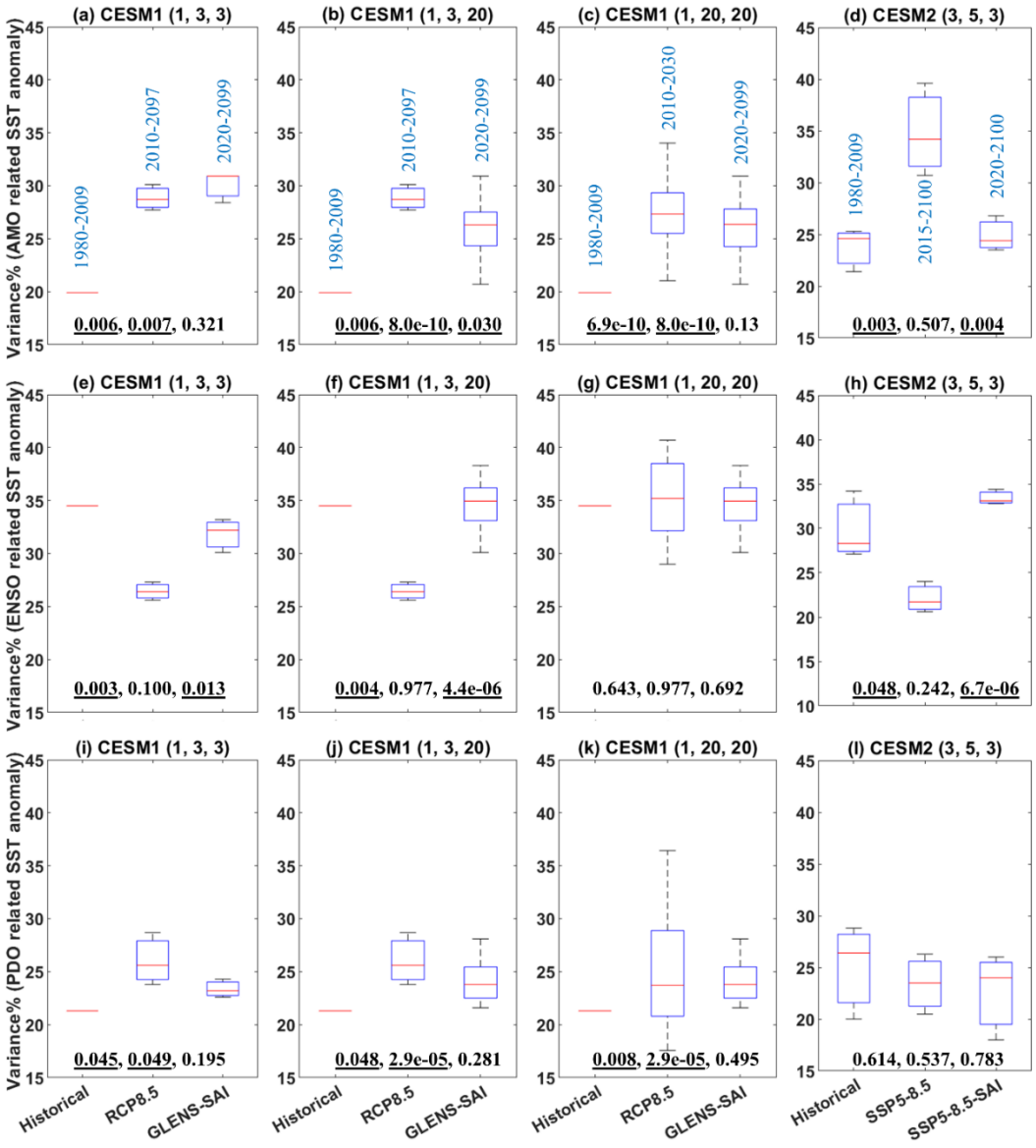

Figure S1. Box and whiskers plot of the variance in the leading EOFs, representing AMO, PDO, and ENSO, relative to the total variance of the SST fields: AMO across the North Atlantic (top row); ENSO (middle row) global SST; and PDO across the North Pacific (bottom row). The values in blue on each column box show the period of the data for historical, greenhouse gas (i.e., RCP-8.5 and SSP5-8.5), and climate intervention (GLENS-SAI and SSP5-8.5-SAI) scenarios. The titles of each subplot refer to the CESM version and the number of ensembles used in the historical, greenhouse gas (RCP8.5 and SSP5-8.5), and SAI (GLENS-SAI or SSP5-8.5-SAI) scenarios, respectively. The median for each experiment is denoted by the red line, the upper (75th) and lower (25th) quartiles by the top and bottom of the box and ensemble limits by the whisker extents. The three values shown in bottom of each sub-plot refer to the p-values obtained from the statistical t-test between historical and global warming, historical and SAI, and global warming and SAI, respectively, in which the underlined values are significant (i.e., $p<0.05$).

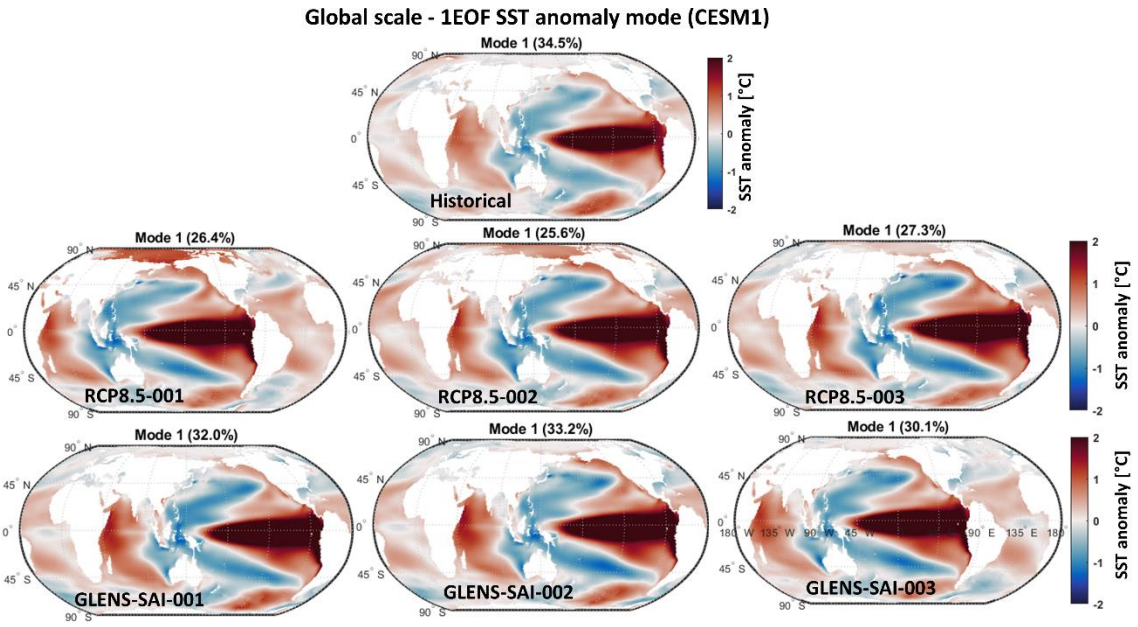

Figure S2. The first EOF (1EOF) modes of global SST anomaly relate to the ENSO index under the CESM1 for the historical data and the three ensemble members (001 to 003) outputs from the RCP8.5 and GLENS-SAI scenarios.

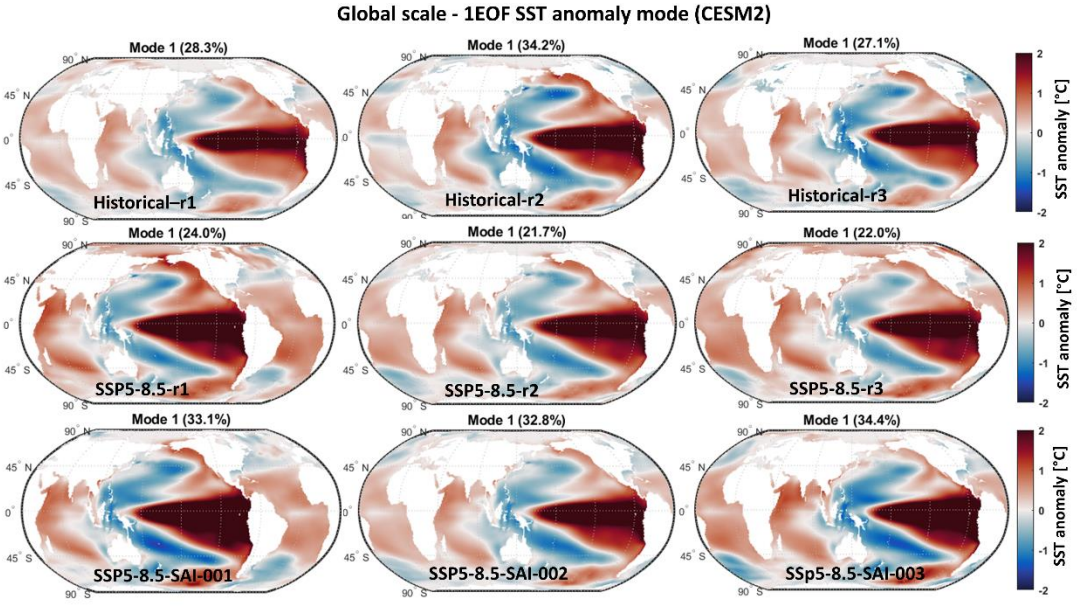

Figure S3. As in Fig. S2, but for the CESM2.

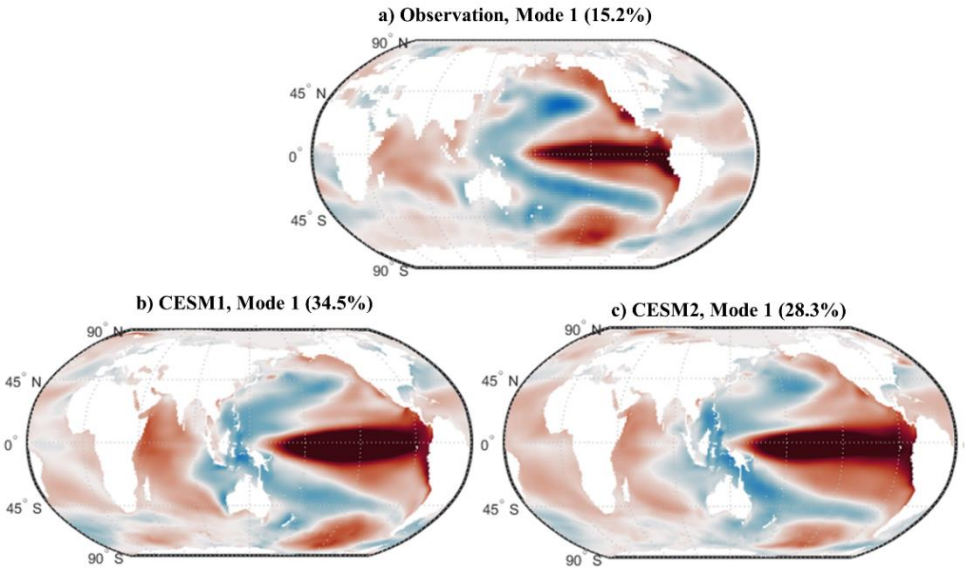

Figure S4. Comparison between spatial leading mode of SST anomaly (related to ENSO) form (a) observation data, (b) CESM1, and (c) CESM2 over the historical 1980-2009 period.

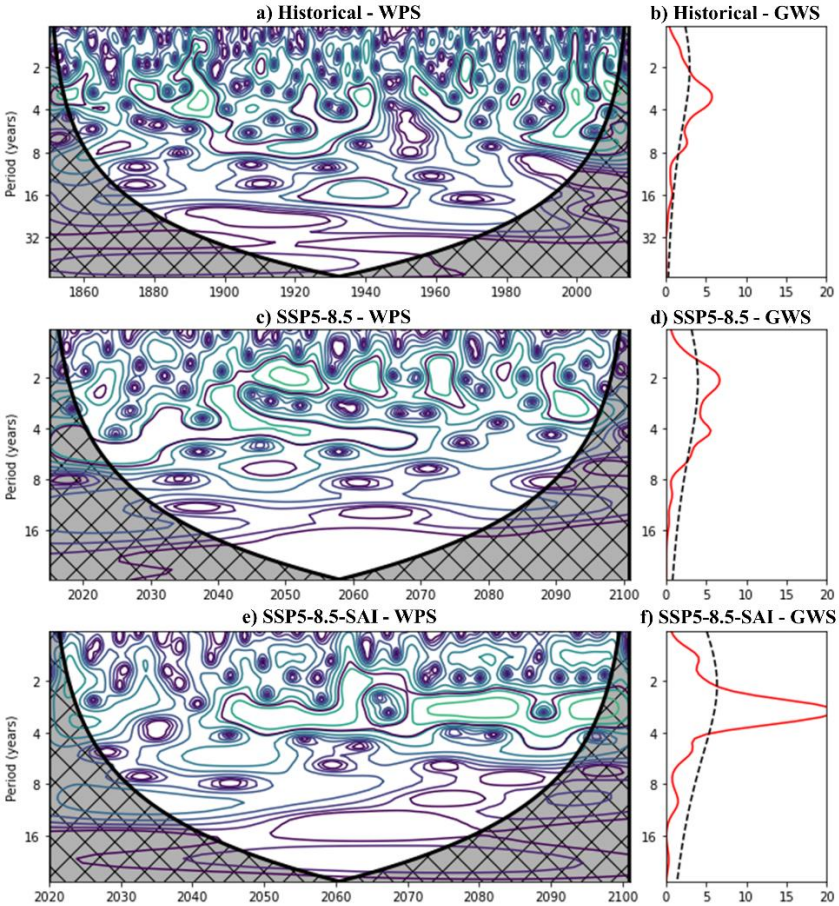

Figure S5. The wavelet power spectrum WPS (left column) and global wavelet spectrum GWS (right column) of ENSO obtained from CWT for the (a and b) historical, (c and d) SSP5-8.5, and (e and f) SSP5-8.5-SAI scenarios.

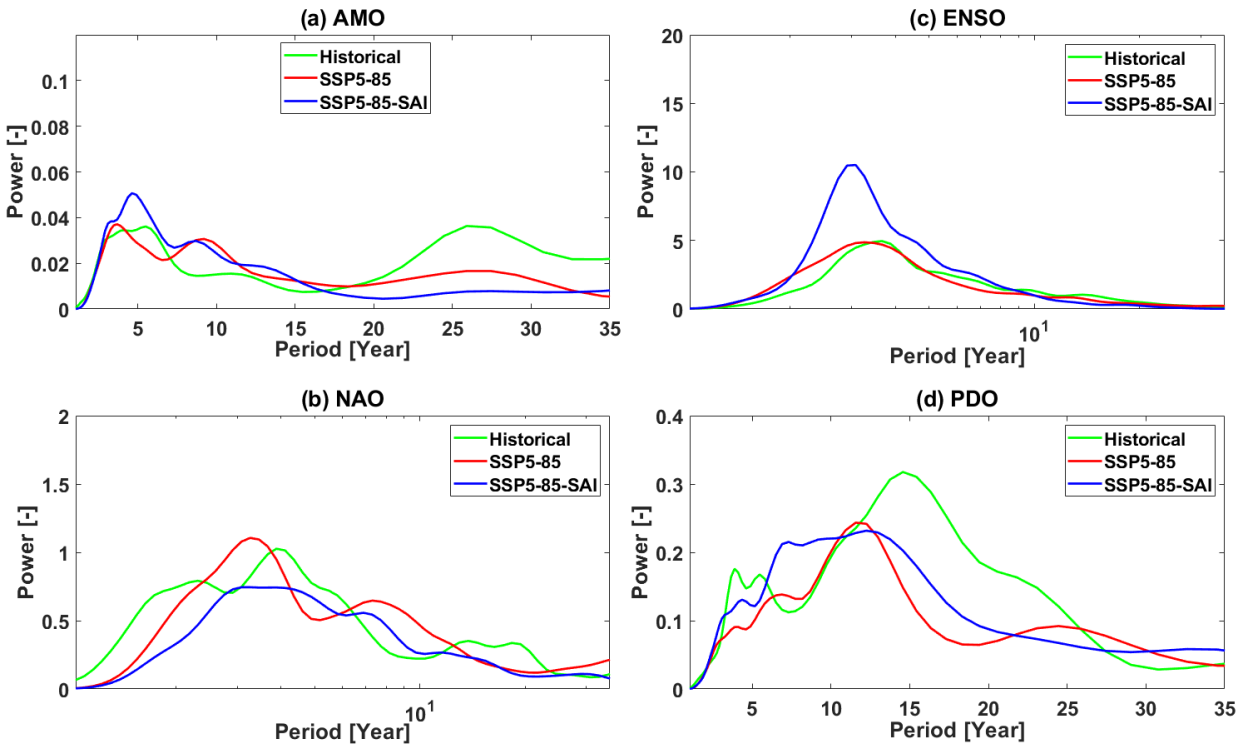

Figure S6. As Fig. 8 but obtained from the concatenated members of the CESM2 historical simulations.

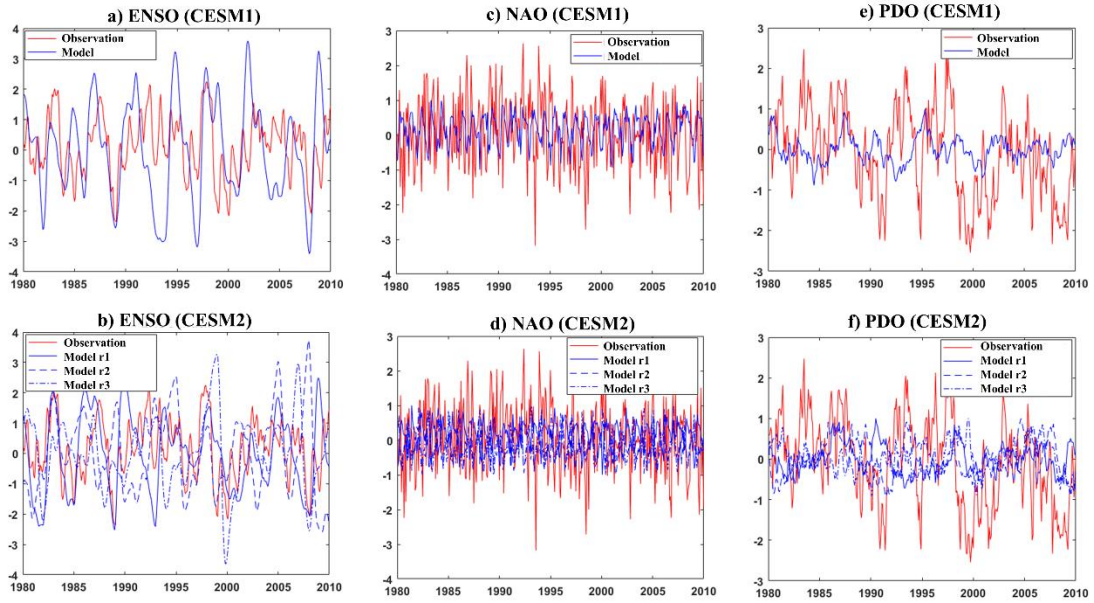

Figure S7. Comparison of the spatial patterns of the first EOF SST ENSO-anomaly from the observations (i.e., measurements) and the CESM1 and CESM2 over the historical 1980-2009 period.